

## Magnetic-Field-Induced Synthesis of Magnetic $\gamma$ -Fe<sub>2</sub>O<sub>3</sub> Nanotubes

Junhong Wang,<sup>†</sup> Yanwei Ma,<sup>†\*</sup> and Kazuo Watanabe<sup>‡</sup>

*Institute of Electrical Engineering, Chinese Academy of Sciences, P.O. Box 2703, Beijing 100080, China and High Field Laboratory for Superconducting Materials, Institute for Materials Research, Tohoku University, Sendai 980-8577, Japan*

Received August 22, 2007

Revised Manuscript Received November 8, 2007

Nanometer-scale magnetic materials and devices are a scientifically interesting and technologically important area of research with many present and future applications in biomedicine, magnetic recording, and spin electronics.<sup>1–3</sup> In particular, considerable effort has been made in the area of one-dimensional (1D) nanostructured materials, such as nanotubes,<sup>4</sup> nanorods,<sup>5</sup> and nanowires.<sup>6</sup> Recently, various approaches, including anodic aluminum oxide (AAO) hard template process,<sup>7</sup> Lecithin soft template,<sup>8,9</sup> and redox methods,<sup>10,11</sup> have been developed for the preparation of these 1D magnetic materials. One of the important classes of 1D nanostructure is magnetic nanotubes. The magnetic properties of these nanotubes can be used to control the formation of their assembled structures, which offers potential applications in biotechnology, nanomedicine, electromechanical system device, etc. However, to the best of our knowledge, there have been few reports about maghemite nanotubes<sup>12</sup> by far. Maghemite ( $\gamma$ -Fe<sub>2</sub>O<sub>3</sub>), which has a cubic spinel structure, is an important material for various applications in industry and technology, e.g., spin electronic devices, high-density magnetic recording, biosensors, and so on.

On the other hand, applications of the magnetic fields for advanced material processing and treatment have been of interest for recent years.<sup>13</sup> It has been demonstrated that martensitic transformation is affected by an external magnetic field when the martensite is a ferromagnetic phase and the

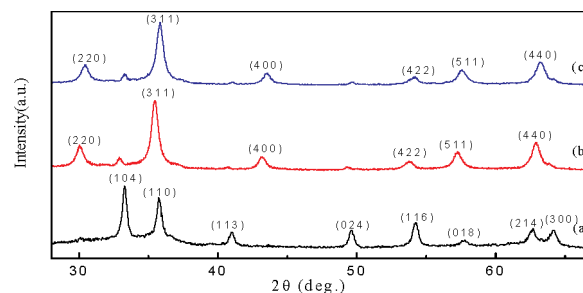


**Figure 1.** XRD patterns of the Fe<sub>2</sub>O<sub>3</sub> samples prepared at 500 °C for 2 h (a) without a magnetic field, and with a 12 T magnetic field: the (b)  $B_{\perp}$  samples and (c)  $B_{\parallel}$  samples.

parent is a paramagnetic phase.<sup>14</sup> Magnetic fields have also been used to create in-plane-aligned membranes of carbon nanotubes (CNTs)<sup>15</sup> and highly conductive and mechanically anisotropic CNTs polymer composites.<sup>16</sup> The alignment of CNTs in magnetic fields arises from the anisotropic magnetic susceptibility of nanotubes. Stronger effects or unknown effects are expected if a high magnetic field is applied during the magnetic nanostructure fabrication process. In this communication, we report a novel method for synthesizing ferromagnetic  $\gamma$ -Fe<sub>2</sub>O<sub>3</sub> nanotubes by a template process with the aid of a high magnetic field. The direction of the magnetic field was perpendicular and parallel to the AAO membrane plane. The products were then termed as the  $B_{\perp}$  samples and  $B_{\parallel}$  samples, respectively. These nanotubes are characterized by structural, morphological, and magnetization measurements.

Figure 1 shows the XRD patterns of the samples prepared at 500 °C for 2 h without a magnetic field and with a 12 T magnetic field. For the samples formed without an applied magnetic field, the XRD pattern well matches that of  $\alpha$ -Fe<sub>2</sub>O<sub>3</sub> (standard cards, JCPDS 33-0664), clearly demonstrating that the as-synthesized samples are a single phase of  $\alpha$ -Fe<sub>2</sub>O<sub>3</sub>. However, XRD patterns of the products produced under a magnetic field are quite different from those of the 0 T samples. For the  $B_{\parallel}$  samples, the XRD pattern is similar to that for the  $B_{\perp}$  samples, although the diffraction peaks for the  $B_{\perp}$  samples seem a little bit narrower. In the case of the  $B_{\perp}$  samples, the major peaks can be indexed to the cubic spinel phase of  $\gamma$ -Fe<sub>2</sub>O<sub>3</sub> with lattice constants  $a = 8.310(1)$  Å. These values are in good agreement with the standard values of bulk  $\gamma$ -Fe<sub>2</sub>O<sub>3</sub> (JCPDS card 25-1402). This result suggests that  $\gamma$ -Fe<sub>2</sub>O<sub>3</sub> has been formed by applying a high magnetic field during processing.

Figure 2 presents SEM micrographs at different magnifications of  $\gamma$ -Fe<sub>2</sub>O<sub>3</sub> samples prepared under a 12 T magnetic field. Obviously, SEM images of the material formed inside the pores showed iron oxide tubes. In the case of the  $B_{\perp}$  samples, a low-magnification view shows a bundle of  $\gamma$ -Fe<sub>2</sub>O<sub>3</sub> nanotubes, and the length is about 30  $\mu$ m (Figure

\* Corresponding author. E-mail: ywma@mail.iee.ac.cn.

<sup>†</sup> Institute of Electrical Engineering, Chinese Academy of Sciences.

<sup>‡</sup> Tohoku University.

- (1) Berry, C. C.; Curtis, A. S. D. *J. Phys. D* **2003**, *46*, R198.
- (2) Zhu, J. G. *IEEE Trans. Magn.* **1993**, *29*, 195.
- (3) Žutić, I.; Fabian, J. *Rev. Mod. Phys.* **2004**, *76*, 323.
- (4) Hu, J. T.; Odom, T. W.; Lieber, C. M. *Acc. Chem. Res.* **1999**, *32*, 435.
- (5) Puentes, V. F.; Krishnan, K. M.; Alivisatos, A. P. *Science* **2001**, *291*, 2115.
- (6) Holmes, J. D.; Johnston, K. P.; Doty, R. C.; Korgel, B. A. *Science* **2000**, *287*, 1471.
- (7) Wang, T.; Wang, Y.; Li, F.; Xu, C.; Zhou, D. *J. Phys.: Condens. Mater.* **2006**, *18*, 10545.
- (8) Kasmi, A. E.; Wallace, J. M.; Bowden, E. F.; Binet, S. M.; Linderman, R. J. *J. Am. Chem. Soc.* **1998**, *120*, 225.
- (9) Imahori, H.; Norieda, H.; Yamada, H.; Nishimura, Y.; Yamazaki, I.; Sakata, Y.; Fukuzumi, S. *J. Am. Chem. Soc.* **2001**, *123*, 100.
- (10) Sudakar, C.; Subbanna, G. N.; Kutty, T. R. N. *J. Mater. Chem.* **2002**, *12*, 107.
- (11) Kandori, K.; Fukuoka, M.; Ishikawa, T. *J. Mater. Sci.* **1991**, *26*, 3313.
- (12) Suber, L.; Imperatori, P.; Ausanio, G.; Fabbri, F.; Hofmeister, H. J. *Phys. Chem. B* **2005**, *109*, 7103.
- (13) Ma, Y. W.; Xiao, L. Y.; Yan, L. G. *Chin. Sci. Bull.* **2006**, *51*, 2944.

- (14) Ma, Y. W.; Awaji, S.; Watanabe, K.; Matsumoto, M.; Kobayashi, N. *Appl. Phys. Lett.* **2000**, *76*, 37.
- (15) Walters, D. A.; Casavant, M. J.; Qin, X. C.; Huffman, C. B.; Boul, P. J.; Ericson, L. M.; Haroz, E. H.; O'Connell, M. J.; Smith, K.; Colbert, D. T.; Smalley, R. E. *Chem. Phys. Lett.* **2001**, *338*, 14.
- (16) Kimura, T.; Ago, H.; Tobita, M.; Tobita, M.; Ohshima, S.; Kyotani, M.; Yumura, M. *Adv. Mater.* **2002**, *14*, 1380.

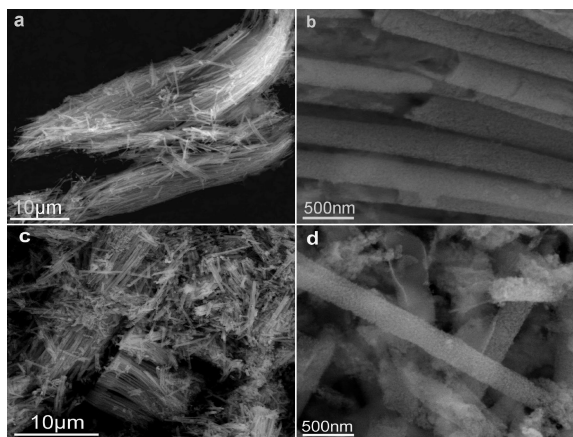


**Figure 2.** Representative SEM images of the magnetic field treating samples. (a) Low-magnification view of the  $B_{\perp}$  samples. (b) Walls of the nanotube bundles. (c) Low-magnification view of the  $B_{\parallel}$  samples. (d)  $B_{\parallel}$  samples at high magnification.

2a). A higher-magnification image reveals that the  $\gamma$ - $\text{Fe}_2\text{O}_3$  nanotubes are arranged roughly parallel to one another (Figure 2b). This demonstrates clearly that magnetic nanotubes can be produced efficiently by the application of magnetic field. For the  $B_{\parallel}$  samples, the lengths of the nanotubes are relatively shorter than those of the  $B_{\perp}$  samples (Figure 2c), and it can also be found that some nanotubes split or crash into individual nanoparticles (Figure 2d), as supported by the broadening of peaks in the XRD pattern. The reason is that the direction of magnetic field is perpendicular to that of fixed action from the AAO template, and when the magnitude of the magnetic force exceeds that of the fixed force from the AAO template, the split of the nanotubes occurs and some nanoparticles are even formed. It is interesting to note that by comparing image a with image c Figure 2, the effect of a magnetic field is different between  $B_{\perp}$  and  $B_{\parallel}$  samples. It seems that the magnetic field works more effectively to produce better  $\gamma$ - $\text{Fe}_2\text{O}_3$  nanotubes when the direction of applied fields was perpendicular to the AAO membrane plane during processing.

To visualize the details inside the  $\gamma$ - $\text{Fe}_2\text{O}_3$  nanotube structures, we performed a HRTEM examination. Figure 3 shows the TEM and HRTEM images of the  $\gamma$ - $\text{Fe}_2\text{O}_3$  sample taken after it was released from the template and dispersed on a Cu grid. In Figure 3a, magnetic nanotubes only several micrometers long are clearly observed. It should be noted that their lengths are shorter than those examined in SEM images (about  $30\ \mu\text{m}$ ). This is due to the destructive effect of mechanical grinding on the fragile tube during the sample preparation for TEM analysis. Figure 3b presents a typical TEM image of the single nanotube. The center parts appear bright in contrast to the wall, confirming their hollow structure of tubes. It is clear that the wall of the  $\text{Fe}_2\text{O}_3$  nanotube is compact and uniform. Images c and d in Figure 3 show the high-resolution TEM images of the outer and inner wall of the  $\gamma$ - $\text{Fe}_2\text{O}_3$  nanotubes, respectively, in which the nanotube walls have a thickness of ca. 20 nm and the edge is a little ragged, consistent with the SEM observations. From the electron diffraction pattern (inset of Figure 3b) of a single  $\gamma$ - $\text{Fe}_2\text{O}_3$  nanotube, it is obvious that the nanotube

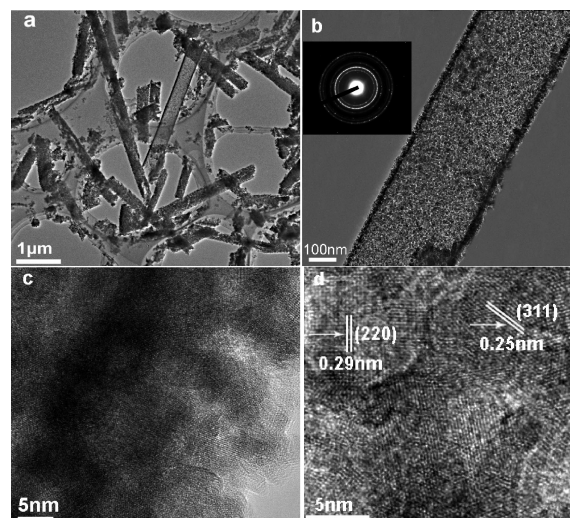


**Figure 3.** (a,b) Typical TEM images of the  $B_{\perp}$  samples. Inset of (b) is the corresponding electron diffraction pattern. (c,d) HRTEM images of the  $B_{\perp}$  samples. The (c) outer and (d) inner walls of a tube.

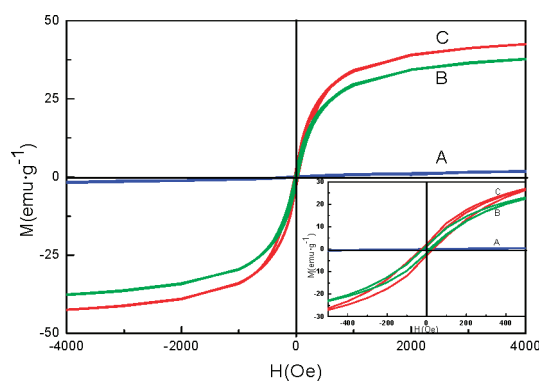


**Figure 4.** Hysteresis loops measured at 300 K for the samples (A) without a magnetic field and with a 12 T magnetic field: (B)  $B_{\parallel}$  samples and (C)  $B_{\perp}$  samples. The inset is the full range of the hysteresis measured between  $-500$  and  $500$  Oe.

has a polycrystalline structure. Furthermore, the wall is composed of multilayered nanoparticles with good crystallinity and several nanometers in diameter. Figure 3d also illustrates the  $\gamma$ - $\text{Fe}_2\text{O}_3$  interlayer spacing of the  $\{311\}$  plane of about  $0.25\ \text{nm}$  and  $\{220\}$  plane of approximately  $0.29\ \text{nm}$ .<sup>17</sup>

To investigate the magnetic properties of  $\gamma$ - $\text{Fe}_2\text{O}_3$  magnetic nanotubes, the hysteresis loops of nanotubes were performed using a SQUID magnetometer. Figure 4 shows room-temperature hysteresis loops of samples prepared with and without the magnetic field after removing the AAO templates. From Figure 4, it is immediately noticed that the samples produced without a magnetic field (A) exhibit room-temperature weak ferromagnetism. However, for the samples annealed in the presence of a 12 T magnetic field, a fully ferromagnetic behavior is observed. For the  $B_{\perp}$  samples (C), the saturation magnetization ( $M_s$ ), coercivity ( $H_c$ ), and remanent magnetization ( $M_R$ ) at 300 K are  $46.1\ \text{emu g}^{-1}$ ,  $28.0\ \text{Oe}$ , and  $2.35\ \text{emu g}^{-1}$ , respectively. The  $M_s$  value is smaller than the corresponding values of the bulk sample

(17) Hyeon, T.; Lee, S. S.; Park, J.; Chung, Y.; Na, H. B. *J. Am. Chem. Soc.* **2001**, *123*, 12798.

( $M_s = 76 \text{ emu g}^{-1}$ ).<sup>18</sup> The deviation is likely due to the nanostructured  $\gamma\text{-Fe}_2\text{O}_3$  and traces of impurity. In addition, the same ferromagnetic character is found for the samples prepared with the field applied along the template plane (B). However, the corresponding values of  $M_s$ ,  $H_c$ , and  $M_R$  are slightly smaller than those corresponding to samples with the field imposed in the perpendicular direction (the  $B_\perp$  samples). This difference can be attributed to the difference in morphology between both samples, as demonstrated by SEM results in Figure 2. Therefore, the above results clearly show that  $\text{Fe}_2\text{O}_3$  samples changed their weak ferromagnetic character at zero field to ferromagnetic behavior at a field of 12 T, in other words, the external magnetic field could be responsible for the formation of  $\gamma\text{-Fe}_2\text{O}_3$  nanotubes.

From XRD results, the sample synthesized in the absence of high magnetic field was indexed to  $\alpha\text{-Fe}_2\text{O}_3$ , whereas the sample prepared with a 12 T magnetic field was verified to  $\gamma\text{-Fe}_2\text{O}_3$  mostly, which indicates that the 12 T magnetic field affected the phase of the samples intensively, because the only difference in preparative methods between the samples is the magnitude of external magnetic field. From a thermodynamic perspective, magnetic field, like temperature, is an independent variable that changes the free energy. Thus, when a magnetic field is applied, the resulting free-energy changes are classified into two terms: the thermal Gibbs free energy,  $\Delta G_T(T)$ , and the magnetic Gibbs free energy,  $\Delta G_M(T, H)$ . Therefore, if a 12 T external magnetic field is imposed during the heating treatment, a new equilibrium will be reached.

It is very common that the product of the thermal decomposition for  $\text{Fe}(\text{NO}_3)_3$  is  $\alpha\text{-Fe}_2\text{O}_3$  without a magnetic field.<sup>19</sup> But, the exact mechanism for the formation of  $\gamma\text{-Fe}_2\text{O}_3$  under the high magnetic field is not completely understood. A possible explanation is that  $\alpha\text{-Fe}_2\text{O}_3$  forms at 500 °C first for the thermal decomposition of  $\text{Fe}(\text{NO}_3)_3$  and then  $\alpha\text{-Fe}_2\text{O}_3$  is transformed to  $\gamma\text{-Fe}_2\text{O}_3$  in the presence of a high magnetic field. Actually, this phase transformation was found earlier by Meillon et al.<sup>20</sup> and Randrianantoandro et al.<sup>21</sup> The total Gibbs free energy of the transformation from  $\alpha\text{-Fe}_2\text{O}_3$  to  $\gamma\text{-Fe}_2\text{O}_3$  can be described as  $\Delta G_T + \Delta G_M$  because of the existence of a magnetic field. Compared to  $\alpha\text{-Fe}_2\text{O}_3$ ,  $\gamma\text{-Fe}_2\text{O}_3$  is metastable. It can be easily transformed to  $\alpha\text{-Fe}_2\text{O}_3$  in the absence of magnetic field at 500 °C,<sup>22</sup>

which indicates that  $\Delta G_T$  is positive. The existence of  $\Delta G_M$  is a result of the difference in magnetic susceptibility between  $\gamma\text{-Fe}_2\text{O}_3$  and  $\alpha\text{-Fe}_2\text{O}_3$ . This energy can be expressed as

$$\Delta G_M = -\frac{1}{2}\mu_0(\chi_\gamma - \chi_\alpha)H^2 \quad (1)$$

where  $\mu_0$  is the permeability of free space,  $\chi_\gamma$  is the magnetic susceptibility of  $\gamma\text{-Fe}_2\text{O}_3$  at a temperature  $T$ ,  $\chi_\alpha$  is the magnetic susceptibility of  $\alpha\text{-Fe}_2\text{O}_3$  at a temperature  $T$ , and  $H$  is the applied magnetic field. At 500 °C,  $\gamma\text{-Fe}_2\text{O}_3$  is ferromagnetic whereas  $\alpha\text{-Fe}_2\text{O}_3$  is antiferromagnetic, because the Curie temperature for  $\gamma\text{-Fe}_2\text{O}_3$  is 590 °C. Therefore,  $\chi_\gamma$  is larger than  $\chi_\alpha$  at 500 °C,<sup>23</sup> which suggests that  $\Delta G_M$  is negative and that the total free energy ( $\Delta G_T + \Delta G_M$ ) is reduced because of the external magnetic field. Therefore, there is a great tendency for the formation of  $\gamma\text{-Fe}_2\text{O}_3$  with the strength of magnetic field ( $H^2$ ). So, magnetic energy is thought to be the driving force for the formation of  $\gamma\text{-Fe}_2\text{O}_3$ . Moreover, it was reported that the magnetic field can enhance the nucleation rate of magnetic materials.<sup>24,25</sup> Thus, we deduce that the presence of the external magnetic field might promote the formation rate of  $\gamma\text{-Fe}_2\text{O}_3$ . As a consequence, the  $\gamma\text{-Fe}_2\text{O}_3$  nanotubes can be obtained when a 12 T magnetic field is applied during the heat treatment.

In summary, we propose the use of a high magnetic field as a viable alternative tool for magnetic  $\gamma\text{-Fe}_2\text{O}_3$  nanotube processing, with the advantages of a simple yet very efficient and contact-free method. Phase identification, microstructure analysis, and magnetic measurements clearly indicate that  $\gamma\text{-Fe}_2\text{O}_3$  nanotubes have been formed under a 12T magnetic field. Such a novel approach to preparing magnetic nanotubes may be very useful for technological applications. To satisfy the application in high-density magnetic recording, magnetic properties of  $\gamma\text{-Fe}_2\text{O}_3$  nanotubes will be improved by the doping of Co or alignment of nanotubes in our further study.

**Acknowledgment.** The authors thank Awaji S., Bai X. D., and Wang H. Y. for their help and useful discussion. This work was supported by the National Science Foundation of China (NSFC) under Grants 50472063 and 50572104 and the “Bairen” program of CAS.

**Supporting Information Available:** Details of sample preparation and characterization method (PDF). This information is available free of charge via the Internet at <http://pubs.acs.org>.

CM702375E

- (18) Cullity, B. D. *Introduction to Magnetic Materials*; Addison-Wesley: Cambridge, 1972; 201.
- (19) Chen, J.; Xu, L.; Li, W.; Gou, X. *Adv. Mater.* **2005**, *17*, 582.
- (20) Meillon, S.; Dammak, H.; Flavin, E.; Pascard, H. *Philos. Mag. Lett.* **1995**, *72*, 105.
- (21) Randrianantoandro, N.; Mercier, A. M.; Hervieu, M.; Grenèche, J. M. *Mater. Lett.* **2001**, *47*, 150.
- (22) Cornell, R. M.; Schwertmann, U. *The Iron Oxides*; Wiley-VCH: Weinheim, Germany, 1996.

- (23) Morin, F. J. *Phys. Rev.* **1950**, *78*, 819.
- (24) Wang, H. Y.; Ma, X. K.; He, Y. *Appl. Phys. Lett.* **2004**, *85*, 2304.
- (25) Zhang, Y. D.; He, C. S.; Zhao, X.; Esling, C.; Zuo, L. *Adv. Eng. Mater.* **2004**, *6*, 310.